
MATSAM: EFFICIENT MATERIALS MICROSTRUCTURE EXTRACTION VIA VISUAL LARGE MODEL

A PREPRINT

Changtai Li^{† 1,2}, Xu Han^{† 2}, Chao Yao¹, and Xiaojuan Ban^{* 1,2}

¹Beijing Advanced Innovation Center for Materials Genome Engineering, University of Science and Technology Beijing, Beijing, China, 100083

²School of Intelligence Science and Technology, University of Science and Technology Beijing, Beijing, China, 100083

January 12, 2024

ABSTRACT

Accurate and efficient extraction of microstructures in microscopic images of materials plays a critical role in the exploration of structure-property relationships and the optimization of process parameters. Deep learning-based image segmentation techniques that rely on manual annotation are time-consuming and labor-intensive and hardly meet the demand for model transferability and generalization. Segment Anything Model (SAM), a large visual model with powerful deep feature representation and zero-shot generalization capabilities, has provided new solutions for image segmentation. However, directly applying SAM to segmenting microstructures in microscopic images of materials without human annotation cannot achieve the expected results, as the difficulty of adapting its native prompt engineering to the dense and dispersed characteristics of key microstructures in materials microscopy images. In this paper, we propose MatSAM, a general and efficient microstructure extraction solution based on SAM. A new point-based prompts generation strategy is designed, grounded on the distribution and shape of materials microstructures. It generates prompts for different microscopic images, fuses the prompts of the region of interest (ROI) key points and grid key points, and integrates post-processing methods for quantitative characterization of materials microstructures. For common microstructures including grain boundary and phase, MatSAM achieves superior segmentation performance to conventional methods and is even preferable to supervised learning methods evaluated on 18 materials microstructures imaged by the optical microscope (OM) and scanning electron microscope (SEM). We believe that MatSAM can significantly reduce the cost of quantitative characterization of materials microstructures and accelerate the design of new materials.

Keywords Materials microscopy image · Microstructure · Image segmentation · Visual large model · Deep learning

1 Introduction

Microstructure recognition based on microscopy image processing and analysis is of great significance for material characterization, performance prediction, and association relationship mining. With the development of automated instrumentation, such as material experimental robots and automatic cutting and grinding machines, and the updates of imaging techniques, the number of microscopy images of materials of different types and modalities is growing exponentially. Material microscopic image processing and analysis is an important part of materials science research. Since material microscopic images can visually demonstrate the morphological features and spatial distribution of the internal structure of materials, establishing the relationship between material microstructural and macroscopic properties has always been a research focus in materials science. As an important basic step, identifying and segmenting the key structures in the image is the key to subsequent quantitative analysis. The accurate and efficient extraction of key organizational and structural features from microscopy images often requires a significant investment of human labor and is subject to subjective factors in manual operation. In recent years, due to the rapid development of deep

*Corresponding author: banxj@ustb.edu.cn. [†]These authors have contributed equally to this work.

learning and computer vision techniques, researchers have developed a series of methods and techniques for materials microscopy images, and corresponding software platforms have successfully integrated these algorithms for use by materials researchers.

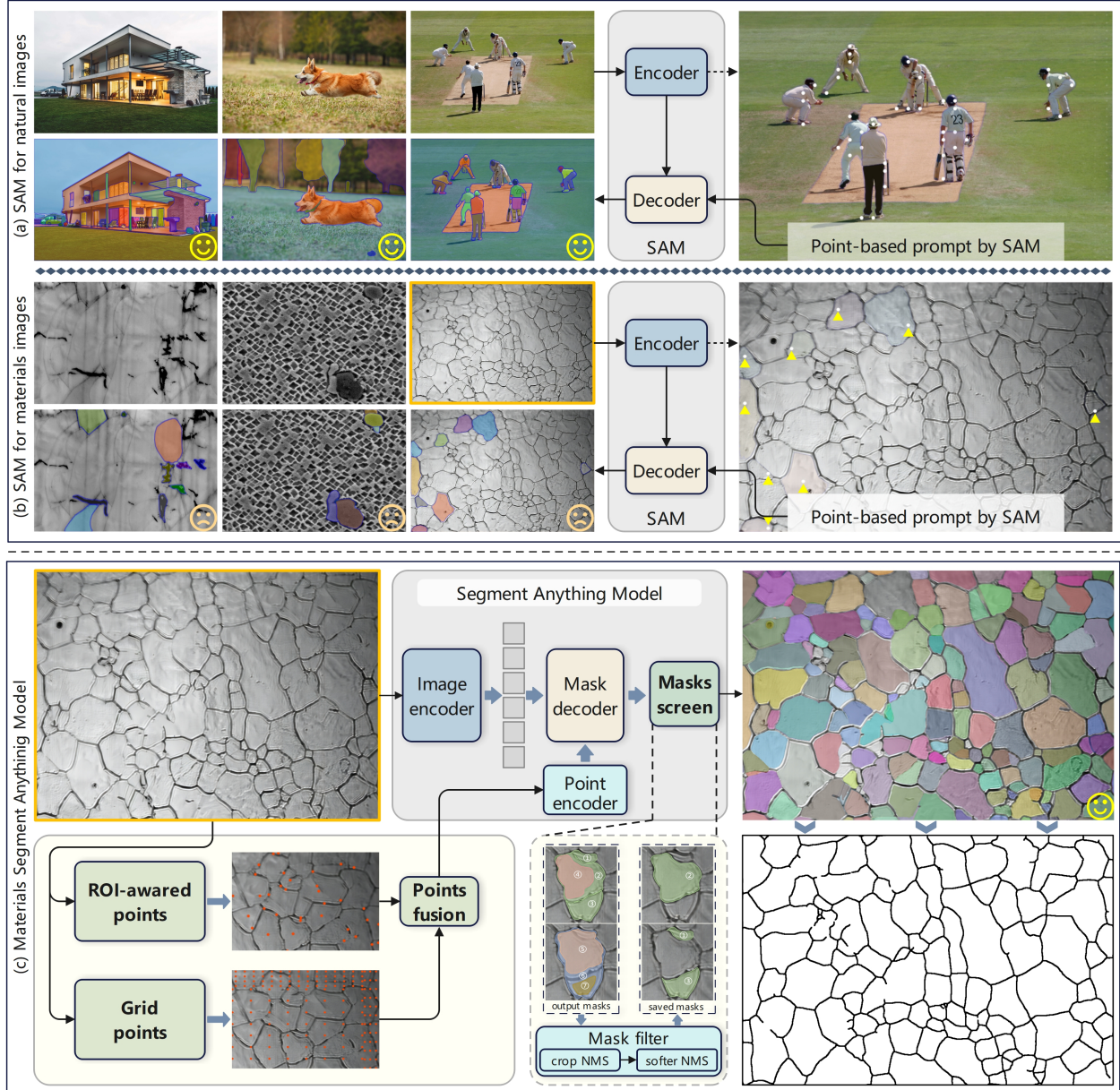


Figure 1: Examples of SAM image segmentation results and the overall architecture of MatSAM. (a) The segmentation results of the native SAM on natural scene images. (b) The segmentation results of the native SAM on three types of material microscopy images. (c) The processing flow and results of MatSAM for material microscopy images.

In the case of simple imaging conditions, clear images, and single structures, traditional image processing methods can produce satisfactory segmentation results through preprocessing, adaptive thresholding, and customized parameters[1]. To some extent, they can meet the practical needs of subsequent quantitative statistical characterization analysis. To achieve accurate segmentation in complex scenes with diverse structures and poor field-of-view conditions, and further improve the reliability of representation, computer vision methods based on machine learning and deep learning have been introduced to the tasks of microscopy image processing and analysis. In general, a specific dataset often requires a large amount of manual annotation to achieve good segmentation results. However, manual annotation is not only time-consuming and labor-intensive but also requires a high level of domain knowledge. In practice, the annotation

results often have a significant number of negative examples, such as inconsistent standards, strong subjectivity, mislabeling, and missing labels. Nevertheless, for deep learning models to achieve accurate segmentation of different microscopic images with multiple materials and structures using a single model, high generalization performance is required. Traditional deep learning models trained on a single dataset make it difficult to achieve this ideal property of cross-material, cross-structure, and cross-modality. The resolution of images obtained from different batches may vary due to factors such as the field of view size and clarity requirements of the original imaging results[2]. Therefore, it is necessary to introduce operations such as field-of-view scaling, region cropping, and size recovery to unify the resolution of the images. These operations introduce additional preprocessing and postprocessing steps, increasing the complexity of the model. Some studies have enhanced the processing capabilities of models by leveraging large-scale pre-training-fine-tuning strategies. Specifically, visual pre-training models specific to material microscopy images have been established using large-scale material microscopy image datasets to achieve accurate segmentation of various microstructures. Stuckner[3] et al. proposed the MicroNet dataset and designed a pre-training strategy for material category classification. In the image segmentation task, migration learning has achieved good test results. Alrfou[4] et al. further validated and explored the image long-range spatial relationship perception ability based on this work by using the ViT (Vision Transformer) architecture. In the pre-training stage, convolutional blocks and Swin transformer blocks are used to jointly learn data features. In the downstream image segmentation stage, the two networks are jointly used as the initial encoders, and their output features are deeply fused. This strategy of using CNN and ViT in both model learning and migration stages can effectively combine the focus of learning of each network and complement each other. However, both methods are based on traditional visual pre-training models, which require further fine-tuning to achieve semantic segmentation of images. Additionally, they cannot achieve truly zero-shot semantic segmentation, which requires cross-structure and cross-modal generalization in zero-shot scenarios.[5]

Segment Anything Model (SAM)[6] is the first general-purpose image segmentation model. Its emergent capabilities and zero-shot knowledge transfer enable new solutions and development paths for computer vision problems. SAM proposes a new image segmentation task called promptable segmentation. The task aims to return reasonable segmentation regions given any prompt information. SAM also builds a massive image data collection and processing engine for collecting and processing large amounts of labeled image data. Under the training of billions of labeled image data, SAM can achieve effects comparable to supervised learning. In addition, SAM has strong zero-shot segmentation capabilities, which can achieve pixel-level identification of new images without additional training. In large language model (LLM) technology[7][8][9], prompt engineering (PE) was initially developed for language models[10]. The constructed prompt words are used as part of the input to the LLM, thus completing a series of specific language tasks. Additionally, the prompt words are not limited to a single modality[11][12]. Text, images, etc. can be encoded as auxiliary information and fused with the LLM. The design and implementation of prompt engineering for different needs is a key factor in the successful application of large models in a variety of tasks and datasets and is also a feasible way for low-cost generalization applications. In addition, different prompt words can lead to vastly different results. Therefore, it is essential to design appropriate prompt engineering.

To explore the processing and analysis capabilities of SAM for material micrograph images, the native SAM model and grid-based prompt words were used to test a variety of material microstructures. The results showed that SAM's automated segmentation function was unable to accurately identify a large number of microstructures in the field of view. This phenomenon can be attributed to the fact that most of the training data for SAM are natural scene images. Compared with material micrograph images, the visual presentation features of the target to be segmented in natural scenes have significant differences. In addition, semantic understanding of material microstructures is more difficult for SAM. **The core problem addressed in this paper is how to adapt SAM to multi-material, multi-structure, and multi-modal material microscopy image datasets, and apply SAM to the accurate identification and extraction of material microstructures that are independent of data at a low cost. Many researchers have attempted to construct domain-specific visual large models based on SAM in medicine and remote sensing imagery.** These efforts have primarily focused on two approaches: (1) Building large-scale datasets within the domain and retraining or fine-tuning the model in its entirety or part. Unlike large language models (LLMs), which can be supported by large-scale datasets with a variety of image-level annotations, it is difficult to construct large-scale datasets with the emergence and zero-shot knowledge transfer capabilities of large models due to the high cost of acquiring image-level annotations. (2) Using SAM's deep feature representation capabilities to design prompt engineering strategies tailored to the characteristics of domain data and combining the two to adapt to domain tasks. This approach has a lower implementation cost and is relatively flexible. Visual large models, such as SAM, have not yet been established in the field of materials science, which involve the construction of large-scale datasets, the design of large-model architectures, and the application of prompt engineering strategies. In this paper, we adopt the second approach and design prompt engineering strategies for common image data in materials characterization.

To address the challenges of multi-material categories, multi-structure, and multi-imaging modes in materials microscopy images, we propose a visual deep learning model solution for materials microscopy images, namely MatSAM (Materials

Segment Anything Model), which is based on the SAM model. MatSAM designs a prompt engineering strategy based on material microstructure shape perception, generating corresponding prompt words for different microscopy images[13][14][15][16]. In addition, MatSAM integrates post-processing methods for quantitative characterization analysis of material microstructure. First, we collected and constructed a total of 13 public and private image datasets, which were imaged by optical microscopes (OMs) and scanning electron microscopes (SEMs). These datasets include a variety of structures, such as common grains, phases, and defects. Second, we designed a prompt fusion strategy for combining interest region key points and grid key points. This strategy is based on the imaging characteristics of material microscopy images and the dense characteristics of key structures in most images. A rule-based image segmentation algorithm is used to extract the coarse-grained key structures in the first step. Based on this result, key points are generated in the region of interest. In addition, to further consider image defects caused by factors such as imaging and manual operations, an adaptive grid keypoint generation strategy is used to enhance the attention to other regions. After the feature extractor of SAM extracts the low-dimensional latent space vector from the original microscopic image, the latent space vector and the fused point hints are jointly input to the decoder of SAM. The decoder upsamples the latent space vector to obtain the closed region of key structures. Then, the multiple closed regions are filtered by the non-maximum suppression (NMS) strategy to obtain the complete microstructural segmentation result.

To verify the effectiveness and generalization ability of MatSAM, we mainly evaluated its micro-structure recognition ability from two dimensions: segmentation accuracy and generalization ability. First, in the scenario without manual annotation, MatSAM has a significant advantage over traditional image segmentation methods in terms of segmentation accuracy. For images with complex micro-structure features, the results of MatSAM segmentation are also viable. In particular, MatSAM achieved the best performance on ten datasets including grain and phase structure, such as PI-1, SS, and DP590-2. Additionally, compared to supervised learning methods (UNet[17], SegNet[18], and TransUNet[19]) that require training, MatSAM achieved comparable or even superior segmentation accuracy on PI-1 and SS datasets with high-quality annotations. On three publicly available datasets with complete annotations, NBS-2, NBS-3[3], and UHCS[20], MatSAM outperforms the supervised methods proposed in the corresponding original paper. Specifically, on the NBS-3 dataset, the IoU score is improved by 0.1938. Second, extensive subjective and objective experimental results demonstrate the generalization ability of MatSAM under different material categories, different microstructure features, and different imaging modalities. Under a variety of conditions, including different categories, imaging quality, and presentation features, MatSAM exhibits good segmentation performance for unseen materials microscopy images, further demonstrating its strong deep feature representation ability. It can be concluded that, for different material microscopy image datasets, by embedding material microstructure shape perception prompt engineering strategies, MatSAM can achieve region segmentation and key microstructure extraction in material microscopy images under zero-label conditions. This is of critical significance for the rapid quantitative characterization of material microstructures in the field of visual large models in materials, thus accelerating the exploration of material structure-property relationships. Currently, strong generalization is becoming a research focus and difficulty in the field of material microscopy image analysis based on artificial intelligence. The application of MatSAM visual large models in the field of materials has opened up new research directions and ideas for this field.

2 Results

In this paper, we first conducted validation experiments on the native SAM for natural scene images and material microscopic images. Figure 1(a) shows the segmentation results of buildings, animals, and crowds, and Figure 1(b) shows the segmentation results of defects, multiphases, and polycrystalline structural features. It can be observed that the main difference between the two lies in the number and distribution of key subject regions. Natural scene images are locally characterized. The number of main regions is small, the semantic features are obvious, and they are mostly concentrated in the center of the image. The overlap between multiple targets is less. In contrast, material microscopic images are globally characterized. They have more key microstructural regions, and the multicrystalline and multiphase structures are dense and dispersed. Due to the diverse geometric shapes of the targets, the overlap between multiple targets is more. **Therefore, directly applying the native SAM to material microscopy images will cause its seed point and mask generation mechanism to fail, resulting in incomplete and inaccurate segmentation results.** This paper investigates the impact of prompt engineering optimization on the generalization of SAM. We propose a material microscopy image analysis method, named MatSAM, which is adaptive to a variety of materials, microstructure features, and imaging modalities. MatSAM optimizes a point-based prompt engineering strategy by leveraging the shape perception of material microstructures, achieving accurate and efficient identification and extraction of material microstructures under unannotated conditions.

2.1 Overall process

MatSAM segmentation workflow is composed of different prompt engineering strategies and a SAM segmentation model. The model takes as input the image to be segmented and the prompts generated by the prompt engineering, and outputs the segmentation mask of the object to be segmented. The segmentation results are then used to extract grain boundaries, precipitates, and impurities. The entire MatSAM method does not require data annotation or model training, and is a zero-shot segmentation method that can directly segment any materials microscopy image. Specifically, MatSAM first generates an appropriate prompt engineering for a given material microscopy image using a point-prompt generation strategy based on material microstructure perception and adaptive grid point methods. The original image and point prompts are then separately encoded in the image encoder and prompt engineering encoder, respectively. The results are then input to the mask decoder to generate corresponding mask segmentation results for each point. In the segmentation process, MatSAM first divides the image into multiple regions and inputs each region into a segmentation model. Then, the multiple masks within each region are processed by region-based non-maximum suppression (NMS) to retain the appropriate results for the same object. Next, the multiple masks between different regions are processed by inter-region softer NMS to retain the appropriate results for different objects without overlap. Finally, all masks are combined and upsampled to obtain the final segmentation results of the material microscopic image.

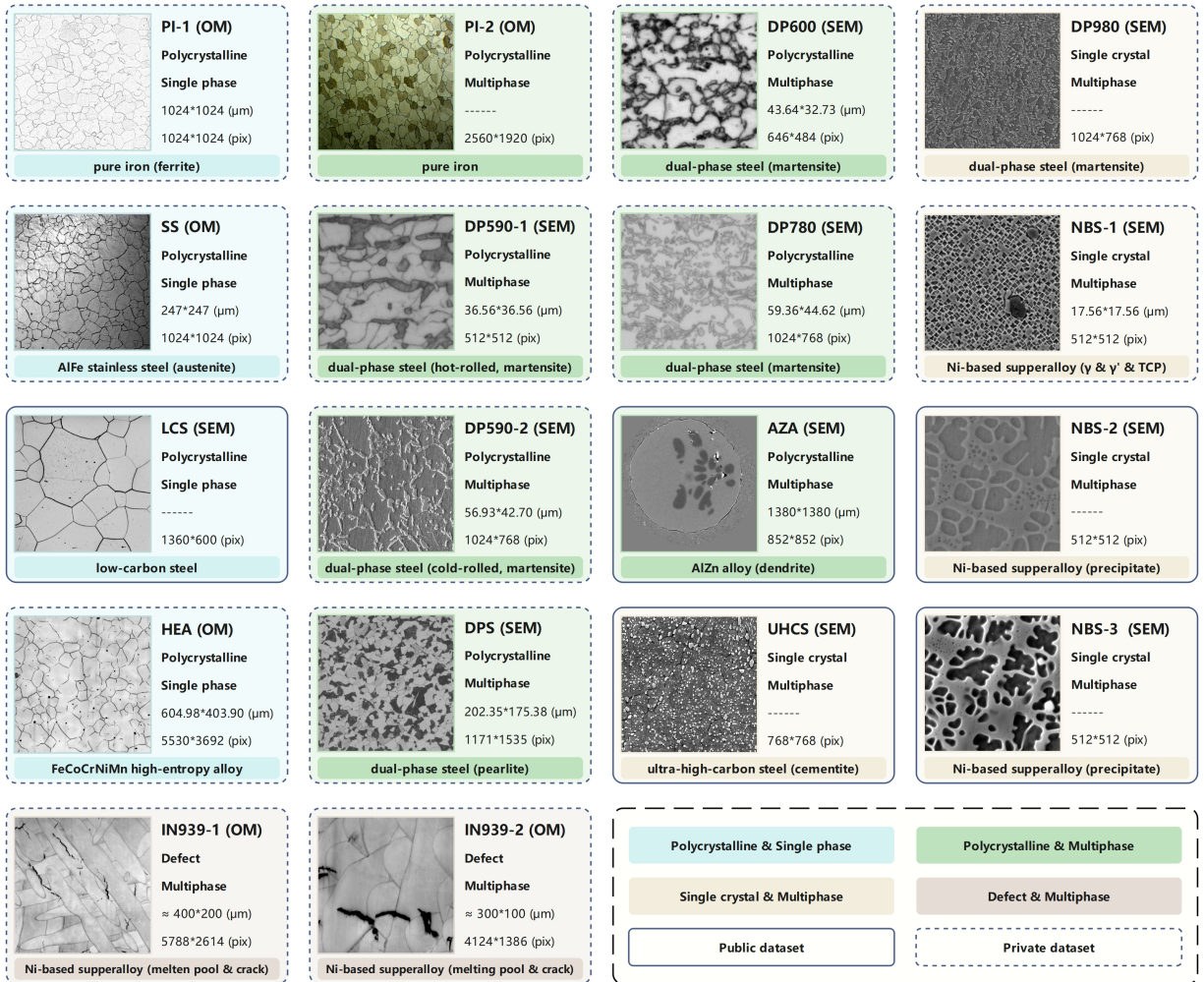


Figure 2: The materials microscopy image dataset used in this paper. The dataset is composed of metal materials, including pure iron, stainless steel, duplex steel, special steel, high-temperature alloy, and high-entropy alloy. The materials are classified into single-phase polycrystalline, multiphase polycrystalline, single-phase polycrystalline, and defects based on the structural features. The imaging methods are divided into optical microscopy and scanning electron microscopy.

2.2 Data sets and evaluation methods

In this paper, we collected 18 public and private material microscopy image datasets to evaluate the zero-shot segmentation performance of MatSAM on different materials, different structural features, and different imaging modalities, thus validating its generalization ability on different types of data. Figure 2 shows a materials card for each dataset. The card contains information such as the material name, dataset abbreviation (imaging modality), single crystal/polycrystal, single phase/multiphase, real size, and image resolution. The colors are used to distinguish different microstructure features. Blue represents single-phase polycrystals, green represents multiphase polycrystals, yellow represents single-phase single crystals, and light brown represents multiphase single crystals with defects. Solid lines represent public datasets, and dashed lines represent private datasets. Metal materials can be classified into pure iron, stainless steel, duplex steel, special steel, high-temperature alloy, and high-entropy alloy based on material category. Based on the characteristics of organizational structure, they can be classified into single-phase polycrystalline, multiphase polycrystalline, multiphase single crystal, and defects. Based on imaging equipment, they can be mainly divided into optical microscopes and scanning electron microscopes.

We propose the MatSAM zero-shot segmentation method and compare it with the traditional rule-based methods and typical deep learning models. We first apply the designed prompt engineering scheme and segmentation model to different types of material microscopy images. Then, we extract the grain structure and phase structure from the segmentation results. Finally, we conduct quantitative and qualitative visual evaluation with the annotated results (except NBS-1 and LCS datasets, all other datasets contain manual annotations). We analyze the subjective and objective performance of the MatSAM zero-shot segmentation method. We mainly compared our method with traditional methods (Canny, OTSU, Watershed) on the PI-1, SS, PI-2, HEA, and DPS datasets that present grain structures. Specifically, on the two datasets with higher annotation quality, PI-1 and SS, we compared our method with supervised learning methods that require training on labeled data, such as UNet, SegNet, and TransUNet, which are based on convolutional neural networks (CNNs) and transformers, respectively. We used three objective evaluation metrics: adjusted Rand index (ARI), F1 score, and recall. The calculation formulas are given in the appendix. The proposed MatSAM method was evaluated on a set of benchmark datasets for biphasic steels, including DP590-1 and DPS, which exhibit phase structures. The performance of MatSAM was compared with that of traditional methods such as OTSU and Adaptive. Additionally, for four publicly available datasets with complete annotations, namely NBS-2, NBS-3, AZA[21], and UHCS, the segmentation results of MatSAM were compared with those of the original papers. The intersection over union (IoU) metric was used as the main objective evaluation metric (the calculation formula is provided in the appendix).

2.3 Polycrystalline dataset segmentation

Multi-crystalline material microscopic image datasets typically consist of a large number of tightly packed grains. Each cross-sectional image contains the grain texture section structure of the corresponding layer. This type of dataset requires the extraction of a binary grain boundary image from the image as the segmentation result.

To evaluate the performance of MatSAM, we conducted experiments on the test set of the PI-1 dataset using MatSAM and several traditional segmentation methods. As shown in Table 1, MatSAM achieved excellent segmentation performance. On 59 test images, MatSAM without post-processing achieved an ARI of 0.8908, while Canny edge detection only achieved an ARI of 0.3312. MatSAM with post-processing also outperformed other unsupervised traditional segmentation methods. Traditional segmentation methods applied to multi-crystalline data have shown that OTSU threshold segmentation is highly sensitive to image grayscale values due to the small grayscale difference between closely packed grains. As a result, the segmentation results often suffer from regional segmentation errors or losses due to grayscale variation. Canny edge detection segmentation is less affected than threshold segmentation and can effectively detect most grain boundaries with significant grayscale differences between grains. However, it is significantly affected by blurred or missing grain boundaries. MatSAM, after receiving a point cue strategy based on material microstructure perception, can provide more accurate prior knowledge of the region to be segmented to the model, resulting in more accurate and refined segmentation results. The high Adjusted Rand Index (ARI) performance on the full-size dataset also demonstrates that MatSAM is capable of handling high-resolution images. Compared to traditional segmentation methods and supervised learning-based segmentation methods, MatSAM’s boundary segmentation results are extracted from the boundaries of each grain object segmentation mask. In other words, MatSAM can directly segment all single-grain object masks. This can be used to accurately count the number of grains and calculate quantitative characterization indicators such as grain perimeter, area, position, and circularity. In the PI-1 dataset, we compare supervised segmentation methods with MatSAM. The results are shown in Table 2. Among the supervised methods, SegNet achieves the best ARI of 0.6325 at full resolution, but is still 23% lower than MatSAM. After standard post-processing, MatSAM is only 6% lower than the best TransUNet in terms of ARI, but outperforms all supervised methods in terms of F1 and recall. This suggests that MatSAM is capable of achieving good performance on the zero-shot segmentation task of material microscopy images. In general, supervised methods

Table 1: Comparison of MatSAM with traditional methods for grain structure segmentation on a dataset of grain structure images.

Dataset	Metric	MatSAM	Canny	OTSU	Watershed
PI-1 (w/o postproc)	ARI↑	0.8902(+0.555)	0.3312	<u>0.3348</u>	0.2108
	F1↑	0.3762	0.3519	0.3541	0.2609
	Recall↑	0.4985	0.3465	0.3261	0.5303
PI-1 (postproc)	ARI↑	0.6336(+0.108)	<u>0.5253</u>	0.2025	0.1979
	F1↑	0.7334	0.6460	0.2571	0.2587
	Recall↑	0.8192	0.8668	0.7802	0.6903
SS	ARI↑	0.5634(+0.195)	<u>0.3684</u>	0.2049	0.1974
	F1↑	0.661	0.4984	0.3574	0.3166
	Recall↑	0.5982	0.4650	0.3721	0.2626
PI-2	ARI↑	<u>0.3467</u>	0.3632	0.1392	0.1803
	F1↑	0.5419	0.5030	0.2179	0.2524
	Recall↑	0.5568	0.7525	0.2032	0.1904
HEA	ARI↑	0.5823(+0.214)	0.3497	<u>0.3682</u>	0.2914
	F1↑	0.4726	0.4182	0.4069	0.3852
	Recall↑	0.4154	0.3258	0.3349	0.3341
DPS	ARI↑	0.4516(+0.017)	<u>0.4348</u>	0.4059	0.3935
	F1↑	0.4805	0.5503	0.5133	0.5114
	Recall↑	0.4093	0.4958	0.4248	0.4363

outperform MatSAM in terms of final segmentation performance, because MatSAM does not undergo any training on a segmentation dataset, but instead performs zero-shot segmentation tasks. MatSAM achieves comparable or even better segmentation performance than supervised methods because of its advantages in data preparation, sampling, and imaging. MatSAM’s strong feature extractor can accurately and effectively segment almost all target regions with the guidance of prior knowledge. Supervised methods, on the other hand, are often limited by the small number of training samples and the small size of the feature extractor parameters. Even after training for a sufficient number of epochs, they may still suffer from performance bottlenecks and overfitting.

Second, we evaluate the performance of MatSAM on a low-quality dataset for zero-shot segmentation. The SS dataset is collected under relatively poor preparation conditions and imaging environments, with much lower image quality than the PI-1 dataset. The images contain more blurry regions, scratches, and impurities. As shown in Table 1, MatSAM achieves an ARI of 0.5634 on 44 test images, while the best Canny edge segmentation method achieves an ARI of only 0.3684. MatSAM has a significant advantage over methods with zero-shot segmentation capabilities. In Table 2, TransUNet achieved the best ARI of 0.6302 among supervised methods, outperforming MatSAM by about 6.7%. This is likely due to the fact that supervised methods can learn the features and annotation characteristics of the data during repeated iterations. This allows the model to avoid regions that are corrupted by impurities, scratches, etc. MatSAM, on the other hand, was not trained specifically for this task. Image blur and impurities are the main factors that affect the segmentation quality. In areas with dark and blurry images and grain accumulation, the model segmentation results have significant errors. However, considering that MatSAM can achieve zero-shot segmentation and extract and analyze the features of individual single-grain objects, such segmentation discrepancies are acceptable.

Additionally, the HEA dataset was prepared with a limited field of view, so each image is composed of multiple regions stitched together. This results in visible horizontal or vertical stitching artifacts in the images. Due to the variation in microscope sampling brightness, there is typically a significant difference in grayscale between the two sides of the artifacts. The image set of HEA is a challenging dataset for grain boundary segmentation because of the presence of a large number of open grain boundaries and protruding cracks. The best segmentation result of traditional segmentation methods is 0.3497 ARI, as shown in Table 1. Supervised learning methods are unable to perform effective

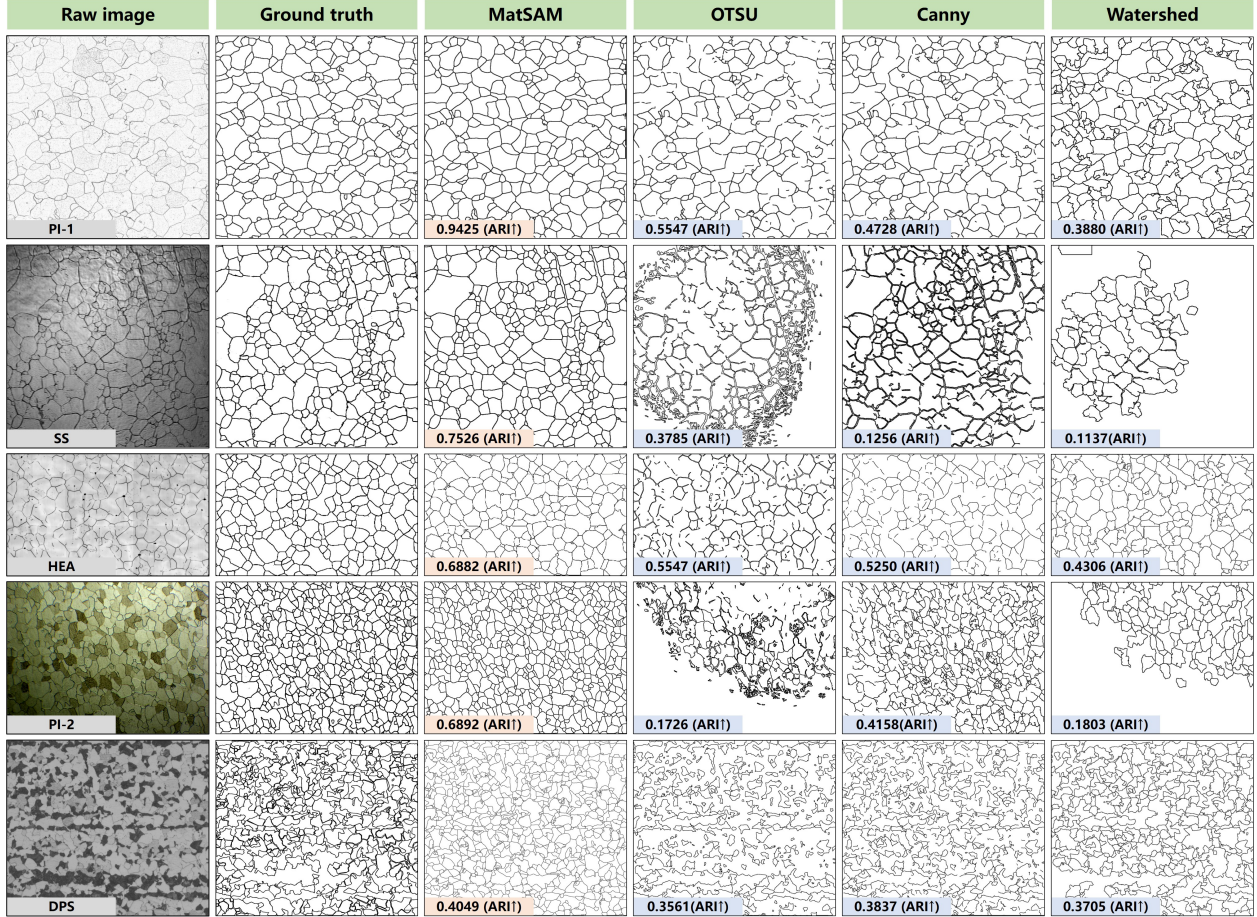


Figure 3: A comparison of MatSAM with traditional rule-based methods on a multi-crystal dataset. The first column shows the original input image, the second column shows the ground truth, and the third to sixth columns show the results of MatSAM, OTSU, Canny, and Watershed, respectively. The corresponding segmentation index ARI is labeled in each result figure, with higher values indicating better performance.

training due to the limited number of images. Using the material microstructure-aware prompt strategy, MatSAM achieved an accuracy of 0.5823 ARI on a high-entropy alloy dataset. Although MatSAM significantly outperforms other segmentation methods, it still produces a large number of segmentation errors. MatSAM performs poorly at most image stitching boundaries, especially in regions with large grayscale differences between the two sides of the stitch. This leads to the re-occurrence of over-segmentation of grain boundaries, resulting in a lower ARI. Another reason for the low ARI is the difference between non-closed grain boundaries and ground truth. As shown in Figure 3, the HEA dataset contains a large number of open grain boundaries. To ensure the completeness of the annotation results, manual annotation is performed along the possible closed paths. However, the segmentation model generates grain boundary results within the visible range. Therefore, in similar open areas, MatSAM may mistakenly segment them into one or more small grain objects. This can lead to the extracted grain boundary results being open or redundant. By using the grain object segmentation mask generated by MatSAM, it is possible to identify and remove grain boundaries that are too distorted at closed boundaries based on the features of the scratch structure. This post-processing method ensures the completeness and smoothness of the segmentation results, and to some extent avoids missegmentation.

In the PI-2 dataset, as shown in Table 1, the best ARI results obtained by the Canny edge segmentation method and the MatSAM algorithm are 0.3632 and 0.3467, respectively. Analysis shows that the performance of both algorithms on the PI-2 dataset is not ideal. The reason is that the light source direction is inconsistent during the data collection process, resulting in uneven image brightness and poor image quality. This makes it difficult to recognize both low-dimensional features such as image grayscale and high-dimensional features such as spatial information. However, the evaluation results could not effectively reflect the ability of MatSAM due to the poor quality of the annotation results. On the DPS dataset, MatSAM performed slightly worse than the Canny method in terms of quantitative indicators, but its subjective

Table 2: Comparison of segmentation performance of MatSAM and supervised methods on PI-1 and SS datasets.

Dataset	Metric	MatSAM	TransUNet	UNet	SegNet
PI-1 (w/o postproc)	ARI \uparrow	0.8902(+0.259)	0.6317	0.5933	<u>0.6325</u>
	F1 \uparrow	0.3762	0.5043	0.5648	0.5441
	Recall \uparrow	0.4985	0.5239	0.5799	0.6242
PI-1 (postproc)	ARI \uparrow	0.6336	0.6957	<u>0.6927</u>	0.6847
	F1 \uparrow	0.7334	0.6453	0.7248	0.7032
	Recall \uparrow	0.8192	0.6182	0.5719	0.5289
SS	ARI \uparrow	0.5634	0.6302	<u>0.5943</u>	0.5336
	F1 \uparrow	0.6610	0.7005	0.6994	0.6443
	Recall \uparrow	0.5982	0.6313	0.6183	0.6091

results were significantly better. Analysis of image annotation quality suggests that due to the presence of numerous errors in the grain boundary annotations, MatSAM’s segmentation results in many regions better fit the grain boundary regions in the original images than the annotations. Therefore, the objective evaluation metrics of its segmentation cannot accurately reflect the ability of the model.

2.4 Multiphase dataset segmentation

Micrograph datasets of multiphase materials contain one or more precipitate phases. Unlike polycrystalline structures, the precipitate phases to be segmented do not typically fill the entire image, but are irregularly distributed throughout the image. Segmentation of this type of dataset requires the extraction of a segmentation mask for the precipitate phases. Different types of precipitate phases typically have significant differences in morphology, structure, and quantity, which can be used to distinguish them.

The DP590-2 dataset contains 21 1024*768 pixel images of precipitates. The main region to be segmented is the martensite precipitates formed during cold rolling, which appear as light white streaks in the images. The IoU of the object mask segmented by MatSAM as the segmentation result is 0.8113, which is significantly higher than the OTSU threshold method (IoU=0.6643). This is a good result for a zero-shot segmentation model, indicating that MatSAM can accurately identify the location and shape of most cold-rolled precipitates. In the region where the model is misclassified, the contrast between the precipitate and the background is small, and the precipitate itself is cut. The former makes it difficult to distinguish the precipitate from the background in the segmentation process, resulting in over-segmentation or under-segmentation. The latter mainly occurs when the precipitate covers the background area, and the precipitate is cut off, making it impossible to effectively extract the entire isolated precipitate structure. In addition, the fine sawtooth shape at the boundary of the precipitate is also a reason for the decline in the fineness of the model segmentation results. Grayscale filtering post-processing can to a certain extent remove the background area that is misclassified. The DP590-1 dataset consists of 23 heat-treated martensitic precipitate images with a size of 512*512 pixels. Compared to cold-rolled materials, the imaging clarity of heat-treated materials is relatively low, and the boundary of precipitates is more blurred, making it more difficult to distinguish. The region to be segmented in the image is the heat-treated precipitate with a low gray value surrounded by a black contour. In traditional segmentation methods, OTSU threshold segmentation achieved the best IoU score of 0.7061. MatSAM, on the other hand, achieved an IoU score of 0.7811. This is because traditional methods are susceptible to local grayscale variations in images, resulting in low detection rates for precipitate phases and misidentification of background regions as precipitate phases. MatSAM, on the other hand, can effectively avoid these interferences, thus improving the segmentation performance of precipitate phases. The MatSAM algorithm is designed to segment individual object masks, which can lead to the misclassification of background regions with shapes similar to precipitates as foreground. This results in the over-segmentation of object masks. A post-processing method based on thresholding can be used to filter out mis-segmented background masks. Additionally, the MatSAM algorithm’s ability to generate individual precipitate object masks provides a reliable basis for subsequent quantitative characterization of precipitates, such as their number, distribution, and area. It is worth noting that MatSAM did not outperform OTSU or Adaptive methods on the four datasets of DPS, DP600, DP780, and DP980. In the DPS dataset, the target phase structure and the foreground have a significant grayscale difference and clear boundaries. After setting an appropriate threshold, the OTSU thresholding method can successfully segment the majority of the darker martensite precipitate phases, with an IoU of 0.9032. MatSAM has a difference of about 6%

Table 3: Performance comparison of MatSAM with traditional methods on the phase structure dataset.

Dataset	Metric	MatSAM	OTSU	Adaptive
DP590-2	IoU↑	0.8113(+0.147)	<u>0.6643</u>	0.2838
	F1↑	0.8333	0.6557	0.1659
	Recall↑	0.8279	0.5775	0.2158
DP590-1	IoU↑	0.7811(+0.075)	<u>0.7061</u>	0.5342
	F1↑	0.8036	0.7334	0.4971
	Recall↑	0.8298	0.8763	0.5198
DPS	IoU↑	<u>0.8403</u>	0.9032	0.5178
	F1↑	0.8802	0.9309	0.4794
	Recall↑	0.8493	0.9402	0.3578
DP600	IoU↑	0.5760	0.7068	<u>0.6190</u>
	F1↑	0.5884	0.7702	0.6671
	Recall↑	0.5716	0.9618	0.7488
DP780	IoU↑	0.4561	0.7686	<u>0.5391</u>
	F1↑	0.5549	0.8627	0.6181
	Recall↑	0.4870	0.8765	0.4881
DP980	IoU↑	<u>0.2772</u>	0.1515	0.4513
	F1↑	0.4340	0.2173	0.5507
	Recall↑	0.7263	0.3378	0.7628

IoU compared to it, and it also achieves a relatively good effect. The analysis may be due to the fact that MatSAM has a slight difference in the details of the segmentation at the grain boundary, which leads to a lower IoU. The other three datasets all have the characteristics of blurred imaging and the mixture of precipitate phase and background. The threshold method, due to its simple calculation method, can obtain preliminary results by simply screening the grayscale range at a single point. However, MatSAM, which encodes images in a more complex way, is more affected by the aforementioned problems and performs poorly on this type of data. The reason for this will be further explored in the discussion section of this paper.

Two publicly available nickel-based superalloy datasets, NBS-2 and NBS-3, contain multiple precipitates of significantly different sizes. The third-level precipitates are particularly small and blurry, making segmentation challenging. In this paper, we perform segmentation experiments using MatSAM, Otsu threshold segmentation, and adaptive threshold segmentation (Adaptive). The results are compared with supervised methods from the original paper, as shown in Table 4. On the NBS-2 dataset, MatSAM achieved an IoU of 0.9094, significantly outperforming the supervised method in the original paper (0.7660). MatSAM can accurately segment almost all larger first- and second-order precipitates, and it also performs well at the precipitate boundaries, with no boundary distortion or misidentification. Additionally, MatSAM can correctly identify some smaller third-order precipitates. Due to the small size of the dataset (only 4 images), conventional supervised methods are unable to perform effective training. However, MatSAM can achieve an IoU of above 0.9 under zero-shot conditions, which demonstrates its good generalization performance on multi-level phase structure datasets. The NBS-3 dataset includes challenging samples with very blurry tertiary precipitates. MatSAM achieves an IoU of 0.7878 on these samples, which is higher than the 0.5940 reported in the original paper. Furthermore, MatSAM achieves an IoU of 0.8284 on four images with relatively clear precipitates. However, on the last image (shown in the second row of Figure 6), which contains many small tertiary precipitates that are difficult to identify even by human experts, MatSAM is unable to effectively segment the precipitates, achieving an IoU of only 0.6250. The results show that MatSAM can accurately segment most first- and second-order precipitate phases, but it has poor recognition and segmentation capabilities for third-order precipitate phases. This is mainly due to the fact that MatSAM has not been trained specifically, and lacks the ability to recognize and segment objects with weak features such as grayscale and structure. Additionally, the prompt word strategy is also unable to effectively

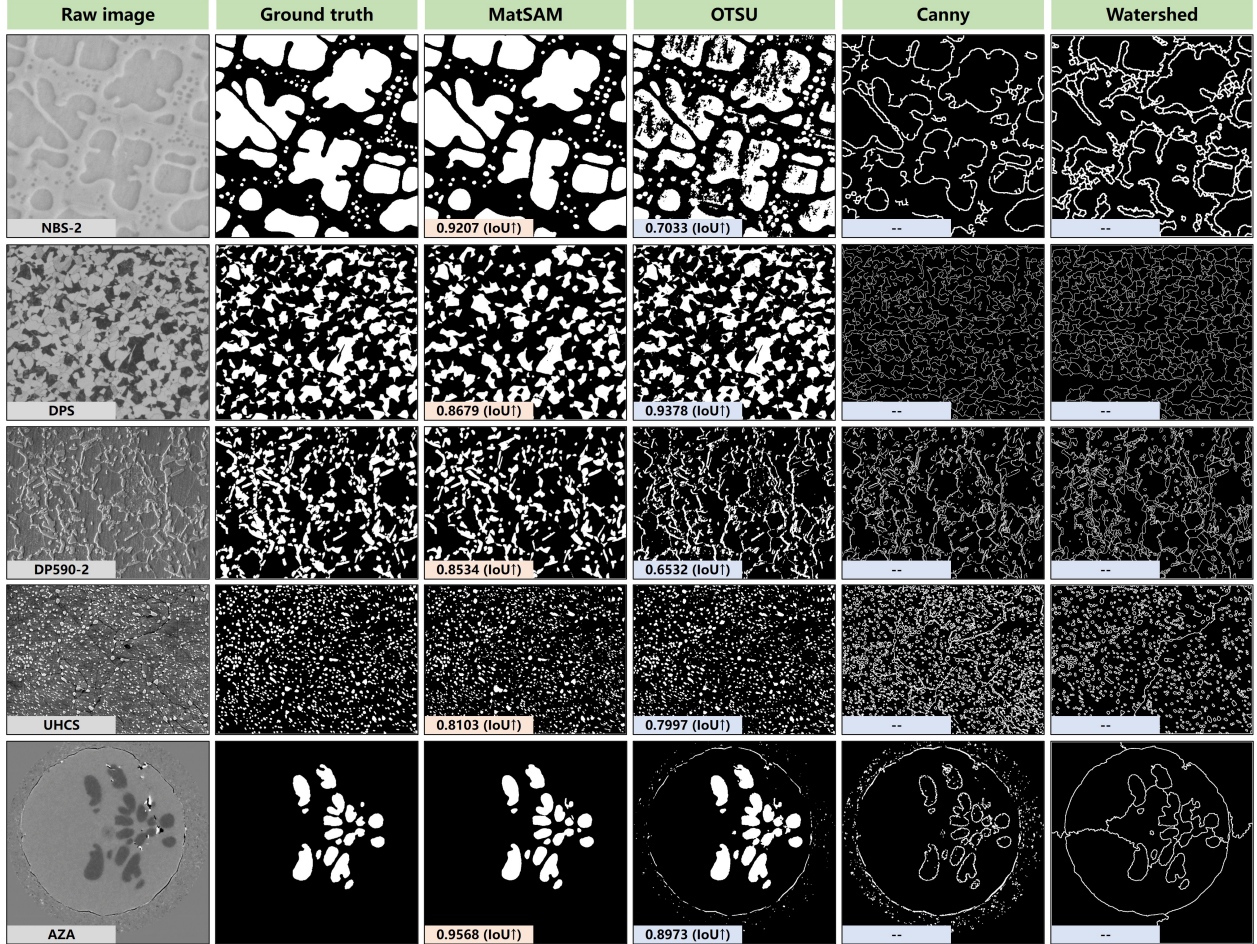


Figure 4: Example of MatSAM versus traditional rule-based methods in a multiphase dataset. The first column shows the original input image, the second column shows the manual annotation, and the third to sixth columns show the output results of MatSAM, OTSU, Canny, and Watershed, respectively. The corresponding segmentation metrics IoU are marked in the results of MatSAM and OTSU (the higher the metric, the better). Since the segmentation results of Canny and Watershed methods are difficult to form effective closed regions, the specific IoU values are not marked.

locate these third-order precipitate phases, resulting in a large number of unsegmented regions in the model. In general, MatSAM still suffers from accuracy issues under extreme conditions. However, the proposed prompt engineering optimization strategy can significantly improve the generalization ability of the model on unseen datasets by integrating prior knowledge of material microstructure shapes. This provides a new and reliable solution for the field of material microscopy image processing and analysis, which often faces challenges such as data scarcity and small sample size.

XCT dendrite data consists of two images, with the foreground to be segmented being the dark precipitate phase in the center of the circular region. MatSAM achieves an IoU accuracy of 0.9578 on the XCT dataset, which is able to accurately segment the precipitate phase, outperforming the OTSU threshold method with an IoU of 0.8853, and approaching the IoU of 0.9690 of the supervised method trained on 30 annotated images by Stan et al.. It is worth noting that Stan et al. identified the best model combination for segmentation after trying 4 pre-training modes, 40 encoder architectures, and 7 decoder architectures. This “search for the best combination” approach is extremely time-consuming, labor-intensive, and computationally expensive, regardless of the dataset used. When faced with different datasets, the model has almost no reuse value and needs to be retrained. MatSAM’s zero-shot segmentation advantages were once again demonstrated, with results that were only 1% lower in IoU at almost zero cost. This good generalization performance underscores MatSAM’s ability to handle diverse datasets. Finally, this paper evaluates MatSAM’s segmentation performance on dense phase-type data. A dataset of spherical particles contains numerous light-colored precipitates that are uniformly distributed on the top surface of a rough alloy crack. The precipitates need to be extracted and segmented. Due to the complex background and large grayscale differences, OTSU performs poorly

on this dataset, with an IoU of only 0.5370. MatSAM, on the other hand, can achieve an IoU of 0.7584, with the vast majority of precipitates correctly identified and segmented.

Table 4: Comparison of segmentation results of MatSAM with other supervised methods on publicly available multiphase datasets.

Dataset	Metric	MatSAM	OTSU	Adaptive	Supervised method
NBS-2	IoU↑	0.9094(+0.143)	0.7516	0.4458	<u>0.7660</u> [3]
	F1↑	0.9544	0.8628	0.5192	/
	Recall↑	0.9390	0.8692	0.3807	/
NBS-3	IoU↑	0.7878(+0.12)	<u>0.6678</u>	0.5171	0.5940[3]
	F1↑	0.8760	0.7957	0.6239	/
	Recall↑	0.8636	0.7873	0.5289	/
AZA	IoU↑	<u>0.9578</u>	0.8853	0.5350	0.9690 [21]
	F1↑	0.9589	0.8803	0.3180	/
	Recall↑	0.9595	0.9729	0.4777	/
UHCS	IoU↑	0.7584(+0.048)	0.5370[22]	0.4595	<u>0.7100</u> [20]
	F1↑	0.7445	/	0.4326	/
	Recall↑	0.7696	/	0.9276	0.8800[20]

3 Discussion

MatSAM is the first known work to apply visual deep learning models to materials microscopy image analysis. Its core idea is to design a prompt engineering strategy that adapts to the features of material microstructures to achieve unsupervised image segmentation. Specifically, MatSAM builds on the SAM model to design a prompt engineering strategy that is based on the shape perception of material microstructures. This strategy fuses the prompts of interest region keypoints and grid keypoints to generate corresponding prompts for different microscopy images. Our results demonstrate that MatSAM, without any training, can achieve significantly better segmentation results than traditional rule-based methods, and can even approach or surpass the performance of supervised learning methods, across images of different materials, structures, and imaging devices. The significance of this capability for material microscopy image processing and analysis tasks is clear. The characterization of material microstructure often requires a great deal of manual intervention. The increasing demand for material research and development, the continuous update of imaging technology, and the rapid increase in the number of devices have all accelerated the generation of microscopy images. For massive microscopy images, even though deep learning and corresponding integrated software packages have somewhat reduced the cost of data processing, traditional models still face the constraints of single-mindedness, poor generalization ability, and the need for accurate labeling. They often need to be modeled for a specific structure of a specific material using a fixed imaging device.

Emergent capabilities (in the training process of deep learning models, a phenomenon sometimes occurs that the model exhibits some functions that were not expected in the training process after the training is completed. These functions are not explicitly introduced in the training process, but are manifested in various forms in downstream tasks) and zero-shot learning are two key features of visual large models, such as SAM. These capabilities are important for the successful application of large models to a wide range of tasks. Benefiting from the powerful deep feature representation ability of SAM for input images, we successfully applied its zero-shot segmentation ability to material microscopy images by designing a prompt engineering. Material microstructures often appear dense in imaging. Additionally, due to the different mechanisms and environments of different imaging devices, it is difficult to unify the descriptions of image quality, resolution, and contrast. In practice, direct annotation of micro-structures in images is often subject to inter-annotator disagreement due to subjective influence, and even significant errors may exist (as shown in the figure). This is not beneficial for model training. Supervised image segmentation tasks inherently learn towards human preferences or high evaluation metrics, rather than being objective. Additionally, on private datasets, the annotations themselves are often not thoroughly reviewed or validated, and the resulting evaluation metrics may not reflect the true capabilities of the model. MatSAM, a material structure analysis method, significantly addresses the inconsistency of

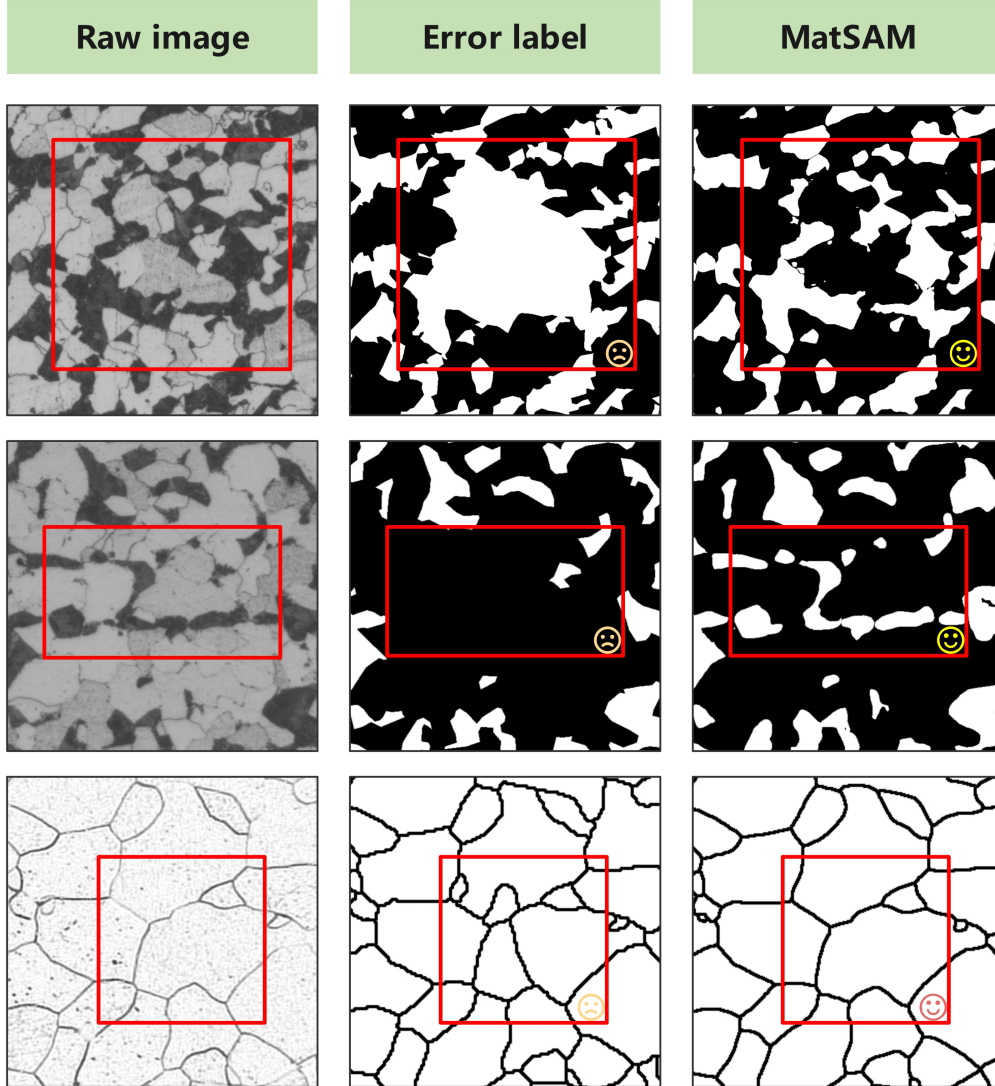


Figure 5: Illustration of mislabeled and missed labels in part of the dataset. The first column shows the original image; the second column shows the mislabeled image; the third column shows the MatSAM segmentation results.

microscopic images of different materials by leveraging point-based cue engineering. It can also produce results that are sufficiently usable.

In this paper, we argue that MatSAM, with its ability to extract material microstructures, can be used as an auxiliary tool in the workflow of material microstructure characterization based on microscopy images. It can significantly accelerate the efficiency of image analysis for researchers. For most normal image segmentation accuracy requirements, the results generated by MatSAM can be directly used for subsequent statistical characterization work. In challenging scenarios where the number of images of a given material to be characterized is large, image quality is poor, and structures are diverse, MatSAM can replace traditional image segmentation methods based on thresholds, gradients, etc., as a pre-segmentation model, to give a more accurate initial result first. Then, through interactive correction involving human intervention, the incorrectly segmented regions are corrected for subsequent model retraining. For example, in the case of continuous three-dimensional slice images of material microstructures acquired by serial sectioning techniques, researchers are more concerned with the three-dimensional characterization results at the layer level. However, the topological relationship restoration of three-dimensional entities between different sections requires higher image segmentation accuracy as a prerequisite for correct tracking and aggregation. It has been statistically shown that it takes about 45 minutes to pre-segment and manually correct a microscope image with approximately 300 grains using traditional segmentation methods. This process is highly susceptible to the subjective biases of the operator. In contrast,

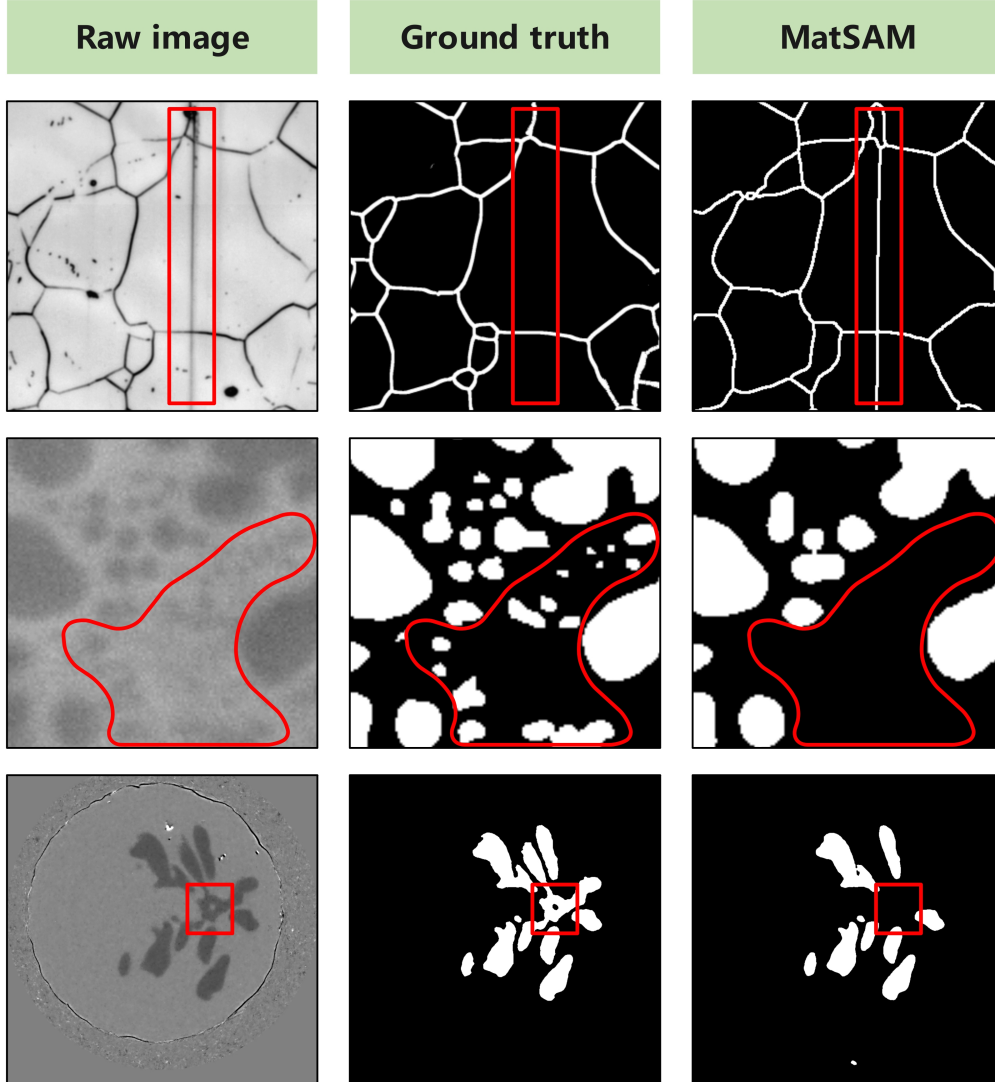


Figure 6: Illustration of undersegmentation and oversegmentation phenomena in MatSAM on some scenes. The first column shows the original image; the second column shows the manual annotation; the third column shows the MatSAM segmentation results.

using MatSAM as a pre-segmentation model can reduce the segmentation time to within 10 minutes. This is because the initial results from MatSAM are already able to accurately identify and segment the vast majority of grains. The operator simply needs to correct the over-segmentation or under-segmentation regions caused by obvious defects or image blurring. This process is less susceptible to visual fatigue and distraction.

It is important to note that, although MatSAM can accurately and efficiently identify and extract microstructural features from microscopy images of a variety of materials, it does have some limitations, as shown in Figure 6: (1) Despite its power, MatSAM still has some limitations. For example, it may fail to identify key structures or oversegment images with significant imaging defects, such as blur, severe stitching artifacts, or very low contrast. (2) In addition, MatSAM may undersegment or missegment images with complex structures, such as those with blurred or even missing boundaries or nested structures. (3) Finally, MatSAM may generate too many proposal points when the input image resolution is too high or the number of ROIs in the field of view is too large. This can increase the computational burden of model inference and prediction. Correspondingly, this paper proposes the following possible future improvements for the current problems of MatSAM: (1) Designing multimodal prompt engineering for visual large models with more knowledge of the materials field. This includes summarizing the types of defects and their formation mechanisms that are likely to occur in microscopy due to both subjective and objective factors. Then, explicit physical modeling

and implicit embedding representation methods are combined to construct additional learnable prompt engineering modules for image defects. These modules can be used to prompt the large model to pay attention to the defect regions that may affect the recognition results through text, image masks, and bounding boxes. This can help to improve the segmentation results and make them more robust to image defects. (2) Visual large model training and fine-tuning for materials microscopy: We perform incremental retraining and fine-tuning of MatSAM’s neural network based on self-supervised learning on a large-scale dataset of materials microscopy images with more material types, structure types, and imaging modalities. This enhances the deep feature representation capability of MatSAM for images in the materials microscopy domain, enabling more reasonable and accurate feature extraction for more complex and diverse materials microstructures. (3) Visual large model lightweight deployment for material-specific needs: Under the premise of ensuring accurate identification of material microstructure, we utilize the techniques of quantization, pruning, and model compression of large-scale deep neural networks to remove redundant parts of the model and retain highly relevant parts for the specific scenario of material microscopy image processing. We also combine model inference acceleration techniques to further optimize the computational efficiency of visual large models, achieving deployment and application under weak computing resource conditions.

4 Methods

4.1 Segment Anything Model

Segment Anything Model (SAM) is a novel large-scale image segmentation model proposed by the Meta AI team. It is trained on a dataset of over 10 million images and 10 billion segmentation masks. SAM has strong zero-shot segmentation capabilities and can be quickly adapted and applied to a variety of downstream computer vision tasks, such as image segmentation. SAM segmentation models are based on prompt engineering. For a given image to be segmented, SAM takes as input a prompt in the form of a point, bounding box, mask, or text. Based on this prompt, SAM generates the corresponding segmentation result. Segment Anything (SAM) is a unified model for zero-shot image segmentation. It consists of three main components: an image encoder, a prompt encoder, and a segmentation mask decoder. The image encoder compresses the input image using a pre-trained vision transformer (ViT), which can handle images of different resolutions. Its global and window attention mechanisms can accurately extract features from the input image, and it outputs a depth feature vector of size $C \times H \times W$. The prompt encoder maps input prompt words of different formats to feature embeddings of 256 dimensions. The mask decoder receives image depth feature vectors and prompt word feature embeddings. First, the image feature is inserted into the prompt word feature to obtain the fused feature. Then, the prompt information is updated to the image depth feature vector again through the cross-attention module (SA) and the layer-by-layer multilayer perceptron (MLP) operation. Finally, the updated feature embedding vectors are transmitted to the transpose convolution and cross-attention layers to generate the final mask segmentation results and the corresponding intersection over union (IoU) and scores.

In this paper, we propose a point-based prompt word method. For a given point set, the prompt word encoder encodes the point set for position encoding and learns an embedding vector to represent foreground or background. After encoding and decoding the image and prompt words, the corresponding target mask is generated. When the generated mask is ambiguous, SAM introduces the "multi-object" approach to provide multiple mask candidates, sorted in descending order of mask scores (up to three). To segment all the objects of interest in an image, SAM provides a set of prompt points that cover as many objects as possible at once. The overlapping regions are then removed using non-maximum suppression (NMS). SAM also provides an automatic mask generation (AMG) method, which can generate a 32×32 grid of equally spaced prompt points over the entire image. This grid is then scaled up by cropping and zooming the original image, to generate a lower-density point grid. The principle of SAM-AMG in generating and screening masks is as follows: the model takes an image and a set of seed points as input. After receiving the image, it first generates multiple rectangular masks of different sizes and overlap ratios. These masks are used to crop the original image into different sizes in different regions. The goal is to perform multi-scale segmentation on the image and produce as accurate and complete segmentation results as possible. We load cropped images of different scales and the corresponding prompt points into the model. We first retain the masks with the highest confidence at each inference. Then, we perform non-maximum suppression (NMS) on the masks retained by multiple prompt points within the cropped frame, retaining non-overlapping segmentation masks within the frame. After all the cropped images are inferred, we integrate all the masks retained by the cropped frames, and then perform NMS between the cropped frames. Finally, we obtain a set of segmentation masks with the highest confidence and no overlap.

4.2 Materials Segment Anything Model

The original SAM method can provide enough points to consider all regions of interest. However, in material microscopy images, key microstructure objects often cover the entire image and are dense and dispersed. Directly using the SAM-

AMG strategy is likely to cause problems such as local missegmentation of grain structures and loss of a large number of objects to be segmented at the edges. The segmentation results are often not ideal. To effectively leverage the strong image deep feature representation capability of SAM with minimal cost and achieve accurate and efficient identification and extraction of key microstructural features in material microscopy images, we propose MatSAM, which is constructed upon the grid-point-based prompt words of SAM.

MatSAM first accurately locates the structures of most target objects to be segmented using threshold pre-segmentation or edge pre-segmentation methods. Then, the generated regular grid of points is adaptively adjusted according to the distribution of material microscopic images. The goal of this is to provide as many “just right” hints as possible, so as to segment all target objects as much as possible, without causing performance degradation or excessive impurities in the segmentation results due to the provision of excessive hints. Specifically, the process of generating prompt points can be divided into two steps. In the first step, a traditional segmentation method (such as Canny edge detection) is used to determine the threshold range of the object to be segmented, and the approximate target region is segmented. Then, abnormal small regions and smooth boundaries are removed by image post-processing methods to obtain several threshold segmentation results. In the second step, the region contour is extracted using the OpenCV and scikit-image image processing libraries, and the centroid point set is obtained as part of the SAM prompt points. In the second step, a suitable number of grid seed points are generated according to the number of the objects to be segmented. Since the threshold pre-segmentation method cannot accurately locate all objects, and the missing objects are often those with inconspicuous pixel differences and difficult to locate shapes. Therefore, it is necessary to retain a proper number of grid seed points to compensate for the omission of the centroid points generated by the threshold method. In addition, the images used for inference are usually cropped from high-resolution images. Therefore, these images often have more dispersed small objects or objects that have been partially cropped off at the edges. This leads to the fact that the generated prompts with the same density in a certain width and height may cover the objects to be segmented with complete shapes in the image, but the same point density at the edges is insufficient to cover the scattered objects to be segmented, resulting in under-segmentation of the results. To address this issue, we propose a novel grid-based segmentation method that adjusts the grid point generation strategy according to the features of the object to be segmented. In the central region of the image, the grid points are generated regularly. However, in the edge region, the grid point generation strategy is dynamically adjusted to provide more dense points, avoiding the segmentation of incomplete objects at the edges.

In addition, MatSAM improves the initial SAM’s selection model cropping frame method. In SAM, non-maximum suppression (NMS) is used to remove redundant masks. Specifically, it ranks masks within the same range by confidence, and then determines whether to keep each mask using IoU as a threshold. This effectively finds the optimal masks for most objects. However, the manually set IoU threshold directly affects the suppression effect of adjacent masks. A too low threshold can easily lead to excessive suppression between objects, making it easy to miss objects in dense scenes. A too high threshold can lead to poor suppression performance and misidentify non-target regions. In this paper, we propose a soft NMS[23] strategy for object detection in material microscopy images. The strategy is based on the work of Bodla et al., which uses a differentiable Gaussian function to compute the penalty value for a mask. The penalty value increases as the intersection-over-union (IoU) between the mask and other masks increases. This strategy is more effective than traditional NMS at reducing false positives and false negatives in dense object scenes.

4.3 Other image segmentation methods

A supervised learning method was used to train a binary semantic segmentation model on a fully annotated dataset. The segmentation model was trained on a single Nvidia RTX4090 24 GB GPU using the PyTorch library. The dataset was split into training, validation, and test sets in a 3:1:1 ratio. All training data in the dataset was randomly horizontally or vertically flipped to improve the model’s robustness to image variations. Prior to training, the model parameters are initialized with a random seed. To ensure the consistency of model training, Adam optimizer and GradScaler gradient scaling are used throughout the training process. This enables the gradients to be learned normally, avoiding the occurrence of gradient explosion or learning stagnation. The learning rate is set to $5e-4$. The loss function uses WeightMapLoss, which is calculated based on the weight map. This is beneficial for the model to learn more accurate segmentation details and mitigate the impact of imbalanced samples. At each epoch, the loss values of the training set and validation set are recorded. The model parameters with the minimum loss value during validation are saved. The training is stopped if the loss value of the validation set in the training remains stable for ten or more epochs. The model with the minimum loss value and without overfitting is selected as the evaluation model. The model architectures used for evaluation include UNet, SegNet, and TransUNet.

Traditional segmentation methods are widely used in material microscopy image semantic segmentation. These methods include threshold-based Otsu segmentation, edge-based Canny operator segmentation, and watershed segmentation. The performance of these methods for binary segmentation tasks is evaluated on a fully annotated dataset. The OTSU

thresholding method is directly affected by the grayscale of the original image to be segmented. Before segmentation, the threshold value needs to be pre-set according to the foreground and background of different datasets. The segmentation objects within the specified threshold range can then be obtained. The boundary results of the segmentation mask can be obtained through post-processing methods such as dilation, erosion, and skeletonization. However, the thresholding method usually has poor details at the boundary intersection, as most datasets have blur, grayscale sudden change, and other situations at the object intersection. The threshold segmentation method will be significantly affected at this point. The Canny edge detection algorithm is also sensitive to grayscale noise, but it performs better in segmenting the edges of grains and phase structures. By setting appropriate operators and thresholds based on the dataset, the algorithm can successfully extract the edge contours of the target object with high accuracy. However, it is easily affected by problems such as boundary blurring and grayscale overlap. Therefore, the application of this method is more sensitive to the influence of the dataset. Watershed segmentation is a segmentation algorithm that uses the image's brightness gradient information. The gradient image can accurately reflect the edges between objects. When there is a clear gap between objects or between the foreground and background, the segmentation results are good. However, when the object edges are blurry, the gradient image cannot accurately reflect the changes in the edges, which can easily lead to inaccurate segmentation. In addition, the overlap or contact between objects will also cause the gradient image to calculate multiple local maxima, resulting in local oversegmentation. To sum up, the performance of traditional image segmentation methods is largely dependent on the quality of the dataset. High-quality datasets with clear images and obvious contrast can achieve better results, while phenomena such as blurred images, stacked objects, and small grayscale differences will significantly reduce the performance of traditional methods.

References

- [1] Boyuan Ma, Xiaoyan Wei, Chuni Liu, Xiaojuan Ban, Haiyou Huang, Hao Wang, Weihua Xue, Stephen Wu, Mingfei Gao, Qing Shen, et al. Data augmentation in microscopic images for material data mining. *npj Computational Materials*, 6(1):125, 2020. doi:10.1038/s41524-020-00392-6.
- [2] Ali Riza Durmaz, Martin Müller, Bo Lei, Akhil Thomas, Dominik Britz, Elizabeth A Holm, Chris Eberl, Frank Mücklich, and Peter Gumbsch. A deep learning approach for complex microstructure inference. *Nature communications*, 12(1):6272, 2021. doi:10.1038/s41467-021-26565-5.
- [3] Joshua Stuckner, Bryan Harder, and Timothy M. Smith. Microstructure segmentation with deep learning encoders pre-trained on a large microscopy dataset. *npj Computational Materials*, Sep 2022. doi:10.1038/s41524-022-00878-5. URL <http://dx.doi.org/10.1038/s41524-022-00878-5>.
- [4] Alexey Dosovitskiy, Lucas Beyer, Alexander Kolesnikov, Dirk Weissenborn, Xiaohua Zhai, Thomas Unterthiner, Mostafa Dehghani, Matthias Minderer, Georg Heigold, Sylvain Gelly, Jakob Uszkoreit, and Neil Houlsby. An image is worth 16x16 words: Transformers for image recognition at scale. *arXiv: Computer Vision and Pattern Recognition, arXiv: Computer Vision and Pattern Recognition*, Oct 2020.
- [5] Changtai Li, Xu Han, Ruohui Jiang, Peiwen Yun, Pengfei Hu, and Xiaojuan Ban. Application and prospects of large models in materials science. *Chinese journal of engineering*, 46(290-305), 2024. ISSN 2095-9389. doi:10.13374/j.issn2095-9389.2023.09.20.002.
- [6] Alexander Kirillov, Eric Mintun, Nikhila Ravi, Hanzi Mao, Chloe Rolland, Laura Gustafson, Tete Xiao, Spencer Whitehead, Alexander C Berg, Wan-Yen Lo, et al. Segment anything. *arXiv preprint arXiv:2304.02643*, 2023.
- [7] Uriah Israel, Markus Marks, Rohit Dilip, Qilin Li, Morgan Sarah Schwartz, Elora Pradhan, Edward Pao, Shenyi Li, Alexander Pearson-Goulart, Pietro Perona, et al. A foundation model for cell segmentation. *bioRxiv*, pages 2023–11, 2023.
- [8] Tal Shaharabany, Aviad Dahan, Raja Giryes, and Lior Wolf. Autosam: Adapting sam to medical images by overloading the prompt encoder. *arXiv preprint arXiv:2306.06370*, 2023.
- [9] Junlong Cheng, Jin Ye, Zhongying Deng, Jianpin Chen, Tianbin Li, Haoyu Wang, Yanzhou Su, Ziyang Huang, Jilong Chen, Lei Jiang, et al. Sam-med2d. *arXiv preprint arXiv:2308.16184*, 2023.
- [10] Rishi Bommasani, Drew A Hudson, Ehsan Adeli, Russ Altman, Simran Arora, Sydney von Arx, Michael S Bernstein, Jeannette Bohg, Antoine Bosselut, Emma Brunskill, et al. On the opportunities and risks of foundation models. *arXiv preprint arXiv:2108.07258*, 2021.
- [11] Chunhui Zhang, Li Liu, Yawen Cui, Guanjie Huang, Weilin Lin, Yiqian Yang, and Yuehong Hu. A comprehensive survey on segment anything model for vision and beyond. *arXiv preprint arXiv:2305.08196*, 2023.
- [12] Xinrun Chen, Chengliang Wang, Haojian Ning, and Shiyang Li. Sam-octa: Prompting segment-anything for octa image segmentation. *arXiv preprint arXiv:2310.07183*, 2023.

-
- [13] Jin Fu, Heng Li, Xu Song, and MW Fu. Multi-scale defects in powder-based additively manufactured metals and alloys. *Journal of Materials Science & Technology*, 122:165–199, 2022. doi:10.1016/j.jmst.2022.02.015.
- [14] Tanishq Gupta, Mohd Zaki, NM Anoop Krishnan, and Mausam. Matscibert: A materials domain language model for text mining and information extraction. *npj Computational Materials*, 8(1):102, 2022. doi:10.1038/s41524-022-00784-w.
- [15] Zhenze Yang and Markus J Buehler. Linking atomic structural defects to mesoscale properties in crystalline solids using graph neural networks. *npj Computational Materials*, 8(1):198, 2022. doi:10.1038/s41524-022-00879-4.
- [16] Shilong Liu, Yanjing Su, Haiqing Yin, Dawei Zhang, Jie He, Haiyou Huang, Xue Jiang, Xuan Wang, Haiyan Gong, Zhuang Li, et al. An infrastructure with user-centered presentation data model for integrated management of materials data and services. *Npj Computational Materials*, 7(1):88, 2021. doi:10.1038/s41524-021-00557-x.
- [17] Olaf Ronneberger, Philipp Fischer, and Thomas Brox. *U-Net: Convolutional Networks for Biomedical Image Segmentation*, page 234–241. Jan 2015. doi:10.1007/978-3-319-24574-4_28. URL http://dx.doi.org/10.1007/978-3-319-24574-4_28.
- [18] Vijay Badrinarayanan, Alex Kendall, and Roberto Cipolla. Segnet: A deep convolutional encoder-decoder architecture for image segmentation. *IEEE Transactions on Pattern Analysis and Machine Intelligence*, page 2481–2495, Dec 2017. doi:10.1109/tpami.2016.2644615. URL <http://dx.doi.org/10.1109/tpami.2016.2644615>.
- [19] Jieneng Chen, Yongyi Lu, Qihang Yu, Xiangde Luo, Ehsan Adeli, Yan Wang, Le Lu, AlanL. Yuille, and Yuyin Zhou. Transunet: Transformers make strong encoders for medical image segmentation. *Cornell University - arXiv, Cornell University - arXiv*, Feb 2021.
- [20] Juwon Na, Se-Jong Kim, Heekyu Kim, Seong-Hoon Kang, and Seungchul Lee. A unified microstructure segmentation approach via human-in-the-loop machine learning. *Acta Materialia*, page 119086, 2023. doi:10.1016/j.actamat.2023.119086.
- [21] Tiberiu Stan, Zachary T Thompson, and Peter W Voorhees. Optimizing convolutional neural networks to perform semantic segmentation on large materials imaging datasets: X-ray tomography and serial sectioning. *Materials Characterization*, 160:110119, 2020. doi:10.1016/j.matchar.2020.110119.
- [22] Brian L. DeCost, Bo Lei, Toby Francis, and Elizabeth A. Holm. High throughput quantitative metallography for complex microstructures using deep learning: A case study in ultrahigh carbon steel. *Microscopy and Microanalysis*, page 21–29, Feb 2019. doi:10.1017/s1431927618015635. URL <http://dx.doi.org/10.1017/s1431927618015635>.
- [23] Navaneeth Bodla, Bharat Singh, Rama Chellappa, and Larry S Davis. Soft-nms—improving object detection with one line of code. In *Proceedings of the IEEE international conference on computer vision*, pages 5561–5569, 2017. doi:10.1109/iccv.2017.593.